High-resolution 3D imaging method using chirped optical frequency combs based on convolution analysis of the spectral interference fringe

doi: 10.1364/OSAC.381540

Research Article Vol. 3, No. 1 / 15 January 2020 / OSA Continuum 20
OSA CONTINUUM

High-resolution 3D imaging method using chirped optical frequency combs based on convolution analysis of the spectral interference fringe

TAKASHI KATO,[1,2] MEGUMI UCHIDA,[1,2] YURINA TANAKA,[1,2] AND KAORU MINOSHIMA[1,2,*]

[1]The University of Electro-Communications (UEC), 1-5-1 Chofugaoka, Chofu, Tokyo, Japan
[2]JST, ERATO Minoshima Intelligent Optical Synthesizer (IOS) Project, 1-5-1 Chofugaoka, Chofu, Tokyo, Japan
[*]k.minoshima@uec.ac.jp

Abstract: We applied an imaging optical system and convolution analysis to a one-shot 3D imaging method with a chirped optical frequency comb to greatly improve the transverse spatial resolution and depth accuracy. We obtained the high contrast spectral interference of a diffusive surface using the designed lens system and developed a simple and robust analysis technique using convolution of an obtained the interference fringe. The developed method was demonstrated to realize submicron-level uncertainty for the depth measurement. When applied to the surface structure of a coin, it demonstrated a transverse spatial resolution of 8.98 lp/mm and depth resolution of 0.35 μm.

1. Introduction

An optical frequency comb (OFC) is an ultrashort pulse train with high controllability and coherence. It has demonstrated a high accuracy and large dynamic range for various point-by-point distance measurements [1–4]. A highly accurate one-shot three-dimensional (3D) imaging method is desired for practical application in various industries. However, it is difficult for existing 3D imaging methods to achieve one-shot 3D imaging with high accuracy and wide range simultaneously. Although the conventional method of laser distance measurement can provide high accuracy [5], it is restricted to stationary objects because the measurement position on the target surface needs to be swept and a delay time is required. Previously, we proposed a principle for one-shot 3D measurement based on ultrafast conversion between the time, frequency, and spatial axis information encoded in chirped ultrashort pulses [6]. However, this method uses a highly chirped supercontinuum and nonlinear optical Kerr shutter realized by an amplified Ti:Al_2O_3 laser because it requires high-power ultrashort pulses. Thus, not only is it impractical but also the measurement performance is limited by the instability of the laser. Because the previous method utilizes isolated pulses, the dynamic range is limited owing to the tradeoff between the degree of chirp and the spectral and temporal resolutions. In terms of practicality, a high-performance and simple measurement method needs to be developed with a practical light source.

Using fiber-based OFCs with excellent stability and practicability, we developed a one-shot 3D imaging method with greatly improved performance [7]. In the previous study, we utilized the spectral interference of chirped ultrashort pulse trains from an OFC to generate spectral images encoded with ultrafast time and space information instead of a nonlinear optical Kerr shutter; thus, a high-power laser was unnecessary. By using the pulse-to-pulse interference of the OFC, the measurement range was greatly extended without losing accuracy, which greatly improved the applicability of the method. Figure 1 shows the principle of the developed one-shot 3D

#381540 https://doi.org/10.1364/OSAC.381540
Journal © 2020 Received 25 Oct 2019; revised 10 Dec 2019; accepted 10 Dec 2019; published 20 Dec 2019

OSA CONTINUUM

imaging method that uses an OFC. It captures spectral interference fringes between chirp pulses (probe) irradiated on the object and chirp-free pulses (reference). Note that we can also choose a chirped pulse as the reference with a relative chirp to the probe because only the relative chirp is important for the proposed method. The spectral interference fringe shows a non-uniform pattern with a minimum fringe frequency at a characteristic wavelength, which indicates that the probe and reference pulses overlap at the wavelength in a chirped pulse. Here, the characteristic wavelength changes with the delay time between the probe and reference. Thus, by measuring the characteristic wavelength as an image, the distance to the target can be measured. Accurately deducing the characteristic wavelength in the spectral interference fringe is important because it greatly affects the measurement uncertainty. In this study, we developed a technique to obtain the characteristic wavelength with high accuracy without complicated analysis, which is suitable for real-time imaging.

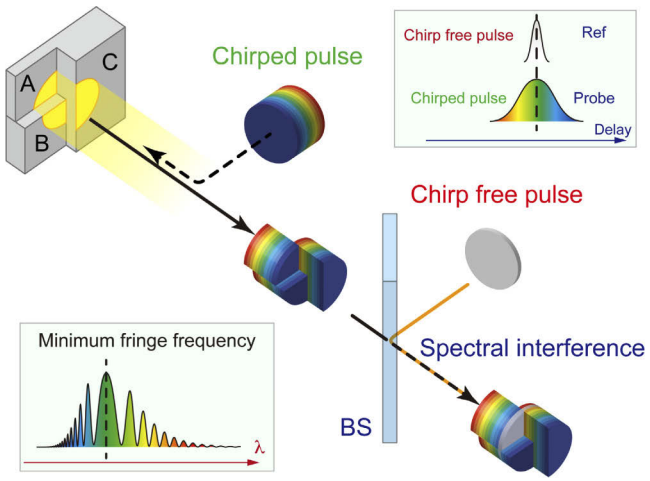

Fig. 1. One-shot 3D imaging method using chirped OFCs.

In our previous study [7], we successfully demonstrated a depth measurement uncertainty on the order of 10 μm for a five-digit dynamic range (i.e., ratio between the resolution (uncertainty) and range). However, many applications demand better depth accuracy at the submicron level as well as better transverse spatial resolution. For the transverse resolution, because the collimated beam is irradiated and its reflected beam is measured, it is only applicable to specular objects and cannot measure complicated shapes with a rough surface. For the depth resolution and accuracy, because the characteristic wavelength that gives the minimum fringe frequency in the spectra is deduced by using the zero-crossing point of the interference fringe, the analysis is not robust against noise and demonstrates a large measurement uncertainty because the calculation process requires differentiation.

An important feature of the developed imaging method is that the transverse and depth spatial resolutions are designed separately. The transverse resolution is determined by the imaging optics setup, and the depth resolution and accuracy are determined by the interference measurement. To demonstrate the capability of the developed method for both the depth and transverse spatial resolutions, which is required to measure minute surface structures, we developed a highly accurate analysis method for detecting patterns in spectral interference fringes that introduces convolution with an imaging lens setup to maintain high measurement accuracy of the interference in the object image.

Various methods have been developed for analyzing the spectral interference fringe in different fields. For example, in multilayer structure measurements with ultrashort pulse, the phase and

OSA CONTINUUM

fringe frequency for the spectral interference fringes of broadband light were obtained with phase unwrapping and the fast Fourier transform (FFT) [8–11]. Some studies theoretically calculated spectral interference fringes of chirped pulses with dispersive media and demonstrated high-precision optical path difference measurements through comparisons with experimental results [12]. The group refractive index of a medium has been measured from the fringe spacing [13] and from phase retrieved and unwrapping of the chirped spectral interference fringes [14]. These studies used the spectral interference fringes because they can be easily measured with a low-speed detector since only the spectrum needs to be measured.

An ideal analysis method would be able to determine the center position of the fringe pattern corresponding to the characteristic wavelength showing the minimum fringe frequency in the captured spectral interference fringe with a low calculation cost and high accuracy. In the present study, we developed a measurement method that accurately detects the center position of the fringe pattern with submicron uncertainty through convolution of the spectral interference fringe. The proposed method uses the bilateral symmetry that exists in the fringe pattern, which gives a strong peak at the center position of the fringe pattern after convolution. This calculation can be performed simply through convolution of the spectrum at each spatial position separately; thus, the depth information can be obtained easily from a single acquired spectral image. In addition, because the data are integrated, the proposed method is robust against signal noise along pixels, unlike the previous method that uses the zero-crossing position.

To achieve a high transverse resolution for one-shot 3D imaging, we introduced an imaging optical system comprising an objective lens and eye lens to focus the probe beam on the measurement object and a matching lens system to adjust the beam diameter according to the reference pulse to generate a high-contrast interference pattern image.

We applied the above two techniques to improve both the depth and transverse spatial resolutions and accuracy. The proposed method was evaluated with a coin and test patterns as measurement objects to demonstrate that one-shot high-precision 3D imaging can be applied to various types of target shapes.

2. Experiment

An experiment was conducted to evaluate the imaging system and convolution analysis. The 3D profiles of the coin and test patterns were measured with a conventional imaging spectrometer and line scanning. Figures 2(a) and 2(b) show the experimental configuration and spectrum and the pulse waveforms of the OFC, respectively. An OFC with a pulse width of 65 fs, center wavelength of 1.55 μm, average power of ∼100 mW, and repetition frequency of 51.06 MHz was generated from an ultrashort pulse train generated by a mode-locked Er-doped fiber laser through an optical amplifier with Er-doped fiber. The repetition frequency (f_{rep}) of the OFC and carrier-envelope-offset frequency (f_{CEO}) were stabilized and controlled by reference to the microwave frequency standard with an Allan deviation of $\sim 10^{-12}$ at a gate time of 1 s. To build the spectral interferometer for the proposed method, the OFC was first divided into reference and probe pulses with a beam splitter. To generate chirped pulses constituting the probe light, we used a 2.5-m-long single-mode fiber (SMF) with a pulse width of 4.2 ps (Fig. 2(b)). The probe pulse then diverged through a planoconcave lens with a focal length of −30 mm and was focused onto the measurement object. The reflected probe pulse from the sample was focused on the imaging spectrometer by an imaging optical system in which a series of lenses was adjusted so that the image of the sample formed on the infrared (IR) camera of the spectrometer. Here, the reference light was a chirp-free pulse. After the delay stage, the reference pulse was overlapped with the probe pulse. After this interference, the pulses were allowed to be incident on the imaging spectrometer (iHR320, HORIBA, Japan), which comprised a reflection-type grating with a groove number of 600 mm^{-1}, and captured with a 640 × 512 pixel InGaAs camera (C12741-03, Hamamatsu Photonics, Japan). The horizontal direction of the captured

image showed the wavelength axis (i.e., depth information), and the vertical direction had the transverse spatial information. Therefore, a spectral image containing two-dimensional shape information was acquired with one pulse. Here, since the exposure time of the camera was 4.6 ms, millions of pulses from the 51 MHz repetition pulse train were averaged. The optical path of the interferometer was adjusted with the delay stage to make adjacent pulses interfere with each other. Thus, the pulse delay time could be adjusted by controlling f_{rep} of the OFC without moving the mechanical stage. Note that we could also measure the pulse-to-pulse interference with any arbitrary pulse in the pulse train. A target object located at any position could be measured by scanning the repetition frequency of the OFC to determine the initial alignment to the position [15]. Once the initial alignment was done, delay scanning was not needed for the shape measurement.

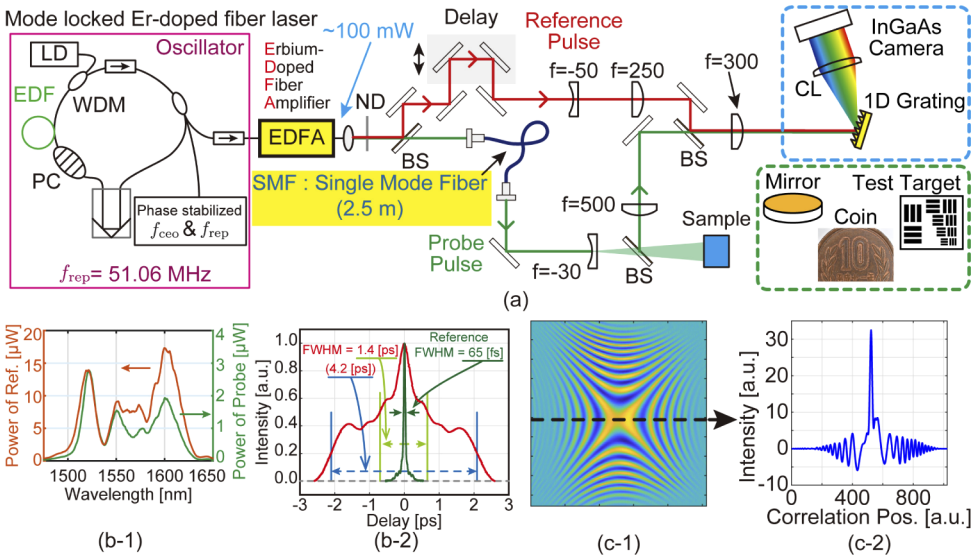

Fig. 2. (a) Experimental configuration (PC: polarization controller, ND: neutral density filter, BS: beam splitter, CL: cylindrical lens). (b) Properties of the OFC: (1) spectrum and (2) pulse waveform of the reference and the probe pulses. (c) Interference fringe analysis method: (1) measured spectral image and (2) convolution of spectral interference between the black dashed line of the left image.

For specular and diffusive shapes, the spectral interference image of the focused probe beam and reference beam needs to be measured. A plano-convex lens with a focal length of 500 mm was placed in the optical path of the probe as the objective length (Fig. 2(a)). A lens with a focal length of 300 mm was placed after the BS to interfere with the reference pulse as an eye lens for focusing on the sample. Finally, the measurement object was captured by the camera of the imaging spectrometer. To make this image interfere with the reference pulse with high contrast, a lens system needed to be placed in the reference optical path to match the beam diameter to the probe image size on the camera. Lens systems with focal lengths of −50 and 250 mm were placed in the reference path, and the distance between the lenses was adjusted so that the beam diameter would correctly correspond to the camera's field angle. With this imaging optical system, the camera could capture the spectral interference image of the sample.

Here, we describe the method used to analyze the position of spectral interference from the captured spectral image. Figure 2(c) shows a schematic diagram of the method for obtaining the interference fringe center position via convolution. First, the convolution was calculated

OSA CONTINUUM

along the wavelength axis (i.e., horizontal direction) of the captured spectral image (Fig. 2(c-1)). Interference fringes have a nearly symmetrical region; thus, the convolution process can emphasize the center position (Fig. 2(c-2)). The convolution signal g is given by

$$g(n) = \sum_{m} f(m)f(n-m) \tag{1}$$

where f is the spectral interference and m and n are indices of the spectral interference and convolution signal data, respectively. The peak position of the convolution signal changes depending on the position of the center of the interference fringe on the wavelength axis, i.e., the shape of the sample. The shape information of the sample was obtained by comparing the peak position to the previously measured calibration curve, which was acquired with the fixed mirror. As a demonstration, we measured a coin's surface and a test pattern to evaluate the transverse resolution of the developed method.

3. Results

Figure 3(a) shows the spectral image obtained when the plane mirror was measured at a delay position of 600 µm. The vertical and horizontal axes represent the space and wavelength, respectively. Figures 3(b) and 3(c) show the analytical results of Fig. 3(a). The cross-sectional fringe was extracted at the spatial position, i.e., vertical axis of 150 pixels (white dash line in Fig. 3(a)), and the convolution was calculated when the delay was changed as shown in Fig. 3(b). The peak of the convolution is plotted in Fig. 3(c). The convolution signal intensity decreased as the convolution signal peak approached the edge of the curve when the convolution was calculated from a spectral image in which a symmetrical fringe pattern was not properly obtained. Therefore, the measurable range was limited to where the convolution signal peak could be distinguished from noise (Fig. 3(c)) and was found to be 741 µm for this experimental system. For convenience, a second-order polynomial approximation was performed to obtain the fitted calibration curve in this range. The calibration curves were created independently for each spatial position, and the wavefront shape, which is dependent on the imaging optical system, was corrected. The residual error between the fitted function and measured value was evaluated to have a standard deviation of 0.35 µm; thus, the measurement was demonstrated to have a submicron level of precision. The depth resolution is more than an order of magnitude better

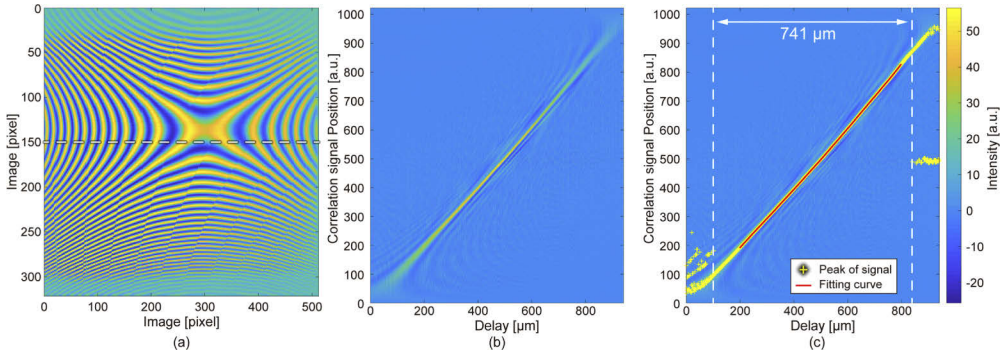

Fig. 3. (a) Spectral image at the delay position of 600 µm (the sample is a plane mirror). (b) Change to the convolution signal with changing delay at 150 pixels (white dashed line in (a)). (c) Peak position of the detected convolution signal (yellow cross). The calibration curve was approximated with a second-order polynomial from the measured peak position (red line).

OSA CONTINUUM

than that of the previous study [7]. To measure an arbitrary object, the depth can be calculated with this calibration curve and convolution peak position.

The 3D shape of a coin was measured via a line scan with the developed method. As shown in Fig. 4(a), although the 3D information was already recorded in a pulse shot as a 2D spectral fringe image, the 1D grating spectrometer could only obtain 1D-position dependent spectrum information in one shot. Therefore, additional 1D position scanning was applied to the sample coin to obtain the full 3D image in this experiment. Even with 1D scanning, the developed method provided rapid and high-resolution 3D imaging, which is already useful for various applications. Total measurement time was 2 min., which was limited by the speed of the stage movement and synchronization with the camera. By use of simple rapid line scanner, the same quality image could be obtained within several second. Moreover, fully no-scanning 3D information could be measured in one shot if 2D spectroscopy techniques such as using a bundle fiber are performed [16]. Figure 4(b) shows the measurement results for the 3D shape of the coin. The XZ plane was measured in one shot and scanned along the Y-axis, and an area of approximately 20 × 23 mm is plotted in Fig. 4(b-1). Figure 4(b-1) shows the surface shape with a depth range of approximately

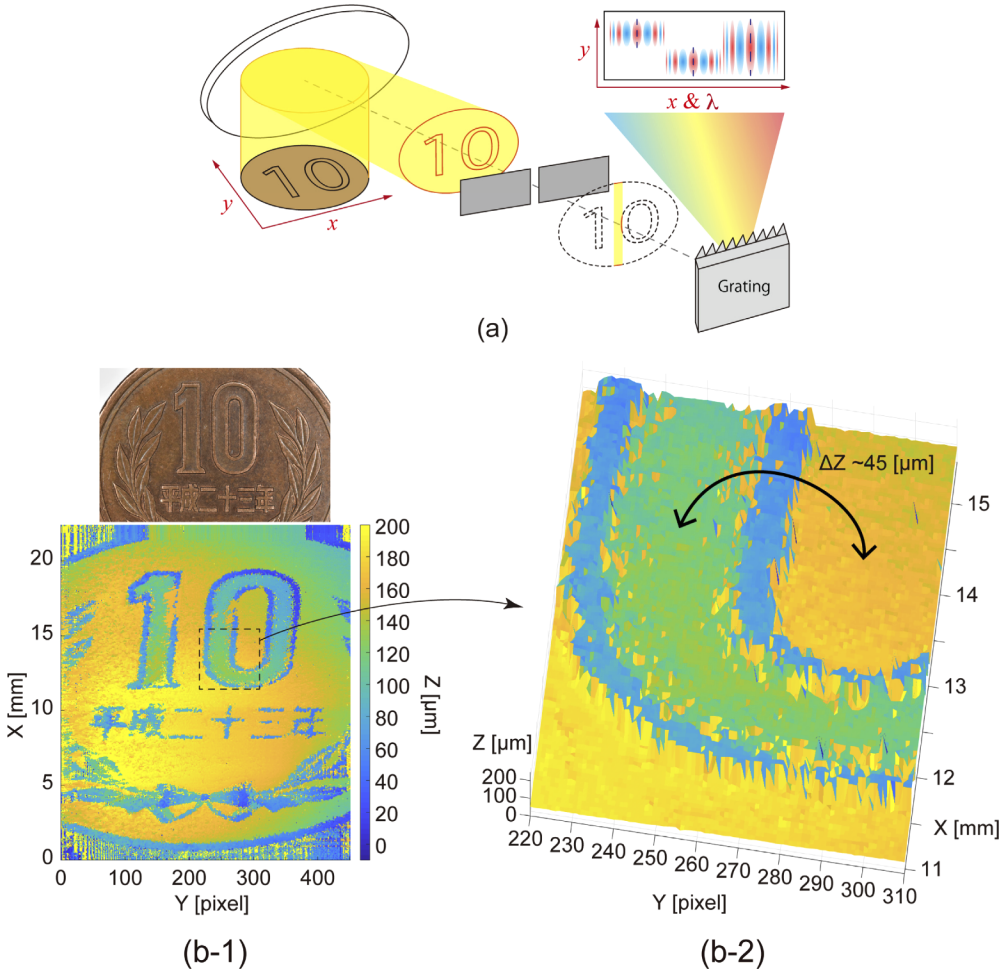

Fig. 4. (a) Imaging spectrometer using diffraction grating and 3D measurement by line scanning. (b) Surface shape of the measured Japanese coin: (1) overview of the structure and (2) fine structure. The coin clearly has a step height of about 45 μm.

OSA CONTINUUM

200 µm. Figure 4(b-2) shows an enlarged image of Fig. 4(b-1), which clearly indicates a fine structure with a depth of approximately 45 µm. These results demonstrate that our developed method can measure rough surfaces with a proper imaging optical system.

Finally, a test chart (1951 USAF) was measured to evaluate the transverse spatial resolution of the proposed method. As a reference, Fig. 5(a) shows native focal images measured at the front slit of the imaging spectrometer and cross-sectional line profiles of each test pattern. These were elements 3 and 4 of group 1 (Figs. 5(a-1) and (a-2)). These images and profiles indicate that the imaging optical setup used in this experiment could visualize the fine structure of the test target. To evaluate the spatial resolution, we plotted a modulation transfer function (MTF) from the visibilities of the line profiles at some elements of groups 1, 2, and 3. The contrast C was calculated as follows:

$$C = \frac{I_{Max} - I_{Min}}{I_{Max} + I_{Min}} \tag{2}$$

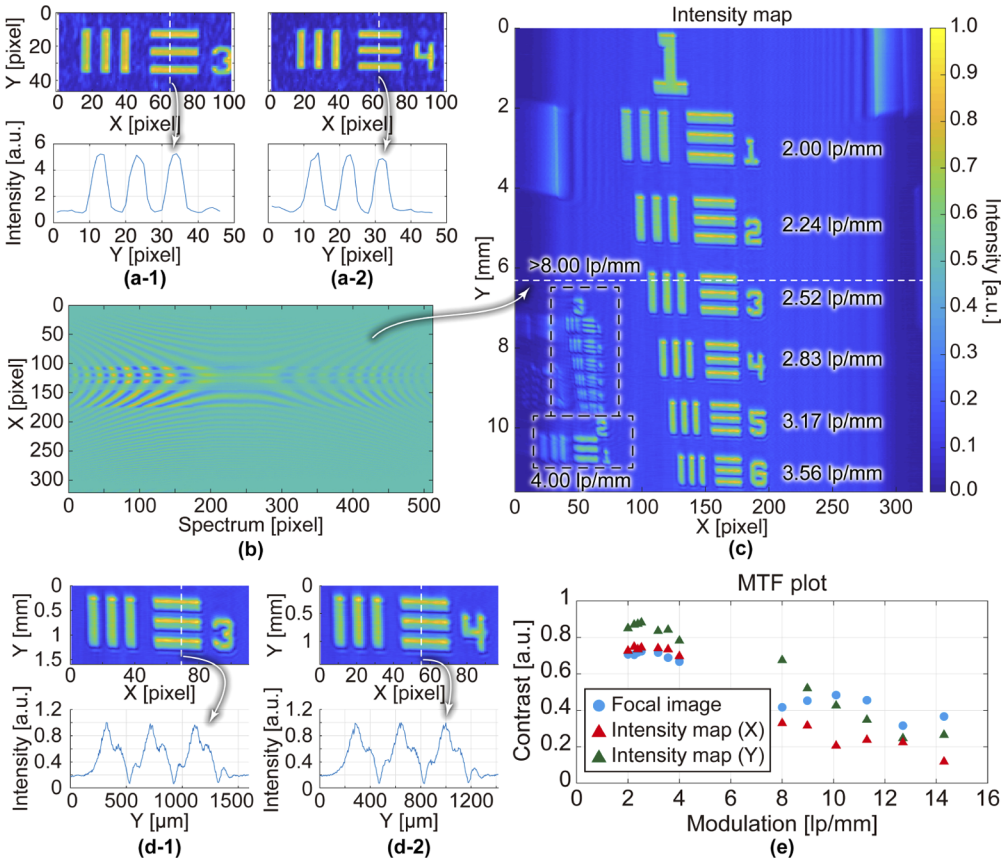

Fig. 5. (a) Focal image at the front slit of imaging spectrometer: (a-1) element 3 and (a-2) element 4 of group 1 (1951 USAF). The green area indicates the gap of the chart. (b, c) Intensity map of the interference image of the test chart (elements of groups 1 and 3 and element 1 of group 2 are shown) obtained with the developed method with a line scan. (d) Enlarged images and 2D profiles of the intensity maps at 2.52 and 2.83 lp/mm, which are same targets of (a-1) and (a-2) (shown in (d-1) and (d-2), respectively). The 2D profiles were obtained from the map on the Y axis and show that the structure at the edge of the chart was deformed by the experimental configuration. (e) MTF plot of the focal image and intensity map obtained by the test chart. The MTF plots of the map on the X and Y axes are shown.

OSA CONTINUUM

where I_{Max} and I_{Min} are the maximum and minimum intensity profiles, respectively, of the test pattern. The MTF of the native focal image is shown in Fig. 5(e) (blue circle).

Figure 5(b) shows the interference image of the test target obtained with the developed method using the chirped OFC with a line scan at the scanning position of 6.30 mm. The scanning direction is represented by the Y axis in Fig. 5(c). To evaluate the transverse spatial resolution for a line scan with the developed method, we plotted a 2D map of the intensity of the obtained spectral interference signal. Figure 5(b) shows that some areas had a high-intensity spectral interference signal because of the reflection from the test pattern. Other areas also had spectral interference, but the intensity was weak because of reflection from the glass plate. Thus, the reflected signal intensity of the metal-coated pattern, which can be distinguished from the glass substrate, indicates the transverse spatial resolution of the proposed method. We calculated the sum of the square of the interference signal along the spectrum axis (horizontal axis in Fig. 5(b)) and obtained the intensity of the spectral interference at each image position (X axis). By an additional line scan in the Y direction, we obtained the 2D intensity map.

Figure 5(c) shows the 2D signal intensity map of the test target obtained with the developed method with a line scan. The map has a resolution of 321 × 2321 pixels, where the size was determined by the pixel resolution of the IR camera and number of line scan steps. The range of the line scan was 11.6 mm with steps of 5 µm. The images on both ends of the measured area were blurred because of the weak interference signal.

Figures 5(d-1) and 5(d-2) show the enlarged image and 2D profile of the 2.52 and 2.83 lp/mm charts, respectively, which were taken from Fig. 5(c). Figures 5(a) and (d) show the same targets. In the experiment, because the plate of the chart was tilted relative to the beam owing to the experimental alignment, the obtained cross-sectional profiles were deformed, which can be seen in the bottom plots of Fig. 5(d) compared to Fig. 5(a). However, the results demonstrated that these test targets were clearly resolved with the developed imaging method.

Finally, we compared the transverse spatial resolutions of the image obtained with the proposed method and the native focal image. Figure 5(e) shows the MTF plots for the cross-sectional images along the X and Y axes together with the native focal images. The MTF plots for the patterns between 4.00 and 8.00 lp/mm are missing because they were out of the range that could be captured at once owing to the limitations of the experimental setup. For the native focal image, the MTF for the target of 8.00 lp/mm was degraded compared to 4.00 lp/mm and reached less than 0.5. Therefore, the spatial resolution of the native imaging optical system was evaluated to be better than 4.00 lp/mm. For the obtained interference image, the MTF for the 8.00 lp/mm along the X axis was worse than that for 4.00 lp/mm and reached less than 0.5, just like the native focal image. However, the obtained interference image along the Y axis showed better values than the native image and reached less than 0.5 at around 10.10 lp/mm. Therefore, the proposed method was evaluated to have spatial resolutions of better than 4.00 and 8.98 lp/mm along the X and Y axes, respectively.

4. Discussion

The convolution analysis acquires the convolution in only one direction for any single image; thus, its calculation cost is very small, and its speed can be easily increased. The analysis is robust against local noise because the signal of the entire fringe pattern is used.

First, we discuss the depth accuracy and measurement range in this study. The measurement range was determined by the pulse width of the reference pulse and probe pulse. The pulse width can be expanded by increasing the amount of chirp. In this experiment, it was adjusted according to the length of the SMF. The range can also be expanded by using a broadband light source because the convolution signal peak position can change greatly. When evaluating the convolution of the fringe pattern, it is important that the specific pattern of the interference fringe should be contained in the spectral image, which severely limits the measurement range.

OSA CONTINUUM

The depth accuracy is determined by the whole spectral bandwidth and wavelength resolution of the spectrometer. As the amount of chirp decreases without the spectral bandwidth changing, the depth accuracy is improved because the convolution position changes more when the distance changes. However, as the amount of chirp decreases, the change rate for the fringe frequency on the wavelength axis also decreases. Thus, the spectral fringe pattern becomes closer to a uniform pattern, i.e., with a single fringe frequency. In other words, the width of the convolution peak increases. In this situation, it is difficult to determine the peak position with high accuracy. If the spectral bandwidth is expanded, the width of the convolution peak became relatively small because the fringe frequency changes rapidly, which makes it easier to determine its position. Thus, the depth accuracy is better when a broad bandwidth and high wavelength resolution are used for detection. The wavelength resolution (or resolution to determine the convolution peak position) can be improved by increasing the number of pixels for the spectral image detection.

Next, we discuss the image resolution (spatial resolution) based on the measurement results of the test chart shown in Fig. 5. As shown in Fig. 5(e), the MTF plot of the native focal image indicates that the contrast decreased between 4.00 and 8.00 lp/mm, which means that it is difficult to capture a fine structure over 8.00 lp/mm with the spectrometer and optical setup used in this study. In addition, the MTF plot of the obtained cross-sectional image along the X axis with the proposed method degraded to below 0.5 at 8.00 lp/mm. However, the MTF along Y axis was better and clearly differed compared to the plot along the X axis. This difference was because the spatial resolutions for the X and Y axes of the image were limited by different factors: the pixel resolution of the IR image sensor in the X direction and the step of the line scan in the Y direction.

The pixel resolution for the image sensor of the IR camera was 20×20 μm. The map on the X axis was focused by the imaging setup in the same way as the focal image. Thus, the MTF plots of the native focal image and interference image along the X axis were the same profile, and both values at 8.00 lp/mm reached below 0.5. On the other hand, we captured the spectral interference image with 5-μm steps in the Y direction. Thus, the obtained image along the Y axis was captured with a finer resolution than that of the IR camera. Considering that the MTF plot of the image in Fig. 5(e) had a higher resolution along the Y axis than along the X axis, we concluded that the transverse spatial resolution of the obtained interference image could reach 8.98 lp/mm, but the experimentally obtained resolution of the X axis was reduced by the pixel resolution of the image sensor. This is because the transverse spatial resolution should be limited by the imaging optical system. Thus, even though the line scan was performed by more finely dividing the focused image, it was impossible to exceed the resolution of the focused image.

In this demonstration, the imaging area was approximately 20×23 mm. However, the field angle was determined by the lens system and can be adjusted by design. The spatial resolution can be also set by the imaging system. For example, with a microscope, the spatial resolution can be increased to the diffraction limit (approximately 0.7 μm when the wavelength is 1.5 μm). In addition, the measurement range can be expanded to greater than a meter by using the pulse-to-pulse interference of the OFC. Thus, it is possible to measure a structure that has a high aspect ratio with a telescope [7,15]. In this case, when an arbitrary optical system is adopted, the mismatch between the wavefronts of the reference and probe pulses should be calibrated by the measurement system for flatness with a reference mirror.

Finally, here we summarize the comparison with conventional spectral interferometric techniques. First, our developed method is not based on the calculation of the precise fringe spacing but is based on the characteristic wavelength region which gives the broadest spacing. Therefore, simple and rapid analysis technique without 2D Fourier transform can be applied as demonstrated in this paper, thus total calculation cost can be reduced. Next, conventional technique based on the fringe spacing has difficulty in applying to a large object, since fine spacing over broad spectral range should be detected and resolved in spectrometer. On the contrary, in our method,

OSA CONTINUUM

we do not need high spectral resolution since we do not need to resolve the fine fringe. Moreover, since we utilized optical frequency comb, pulse-to-pulse interferometry can be applied to a large object with high accuracy. All of these are strong advantages in the developed method even with additional line scan as demonstrated in this work. Finally, as mentioned, with 2D spectroscopic detection techniques, such as fiber bundle, fully no-scanning 3D imaging is achieved.

5. Conclusions

To realize a one-shot 3D imaging method using a chirped OFC for measuring arbitrary shapes, we introduced a simple convolution analysis method to the imaging optical system for improved accuracy. We experimentally verified the effectiveness with line scanning and a spectrometer. The experimental results demonstrated that highly accurate measurements were realized with a depth resolution of 0.35 μm, and the surfaces of a coin and test charts were measured with an imaging optical system at a spatial resolution of 8.98 lp/mm. This can be increased up to the diffraction limit by changing the imaging setup. We demonstrated that a general-purpose imaging spectrometer can be used to acquire a 3D shape with a simple line scan. This method already provides simple and practical 3D imaging. Moreover, because the whole 3D information of the object shape is already recorded in an ultrashort pulse of the OFC, a 3D shape can be simultaneously acquired without scanning by 2D spectroscopy using a bundle fiber [16] or 2D diffraction grating. Because 3D shape information can be stored in any ultrashort pulse in the OFC, dynamic phenomena such as ultrafast (e.g., femtosecond) transient phenomena and fracture phenomena can be measured simultaneously with a submicron level of spatial uncertainty. Because the proposed analysis method does not require high computing power, it can contribute to the development of convenient one-shot 3D imaging systems that use small interferometers and electronic devices.

Funding

Japan Science and Technology Agency through the ERATO Minoshima Intelligent Optical Synthesizer (IOS) Project (JPMJER1304); Japan Society for the Promotion of Science KAKENHI (17K17727, 19K15464).

Acknowledgments

The authors thank Dr. Yoshiaki Nakajima for his help with the laser stabilization.

Disclosures

The authors declare no conflicts of interest.

References

1. K. Minoshima and H. Matsumoto, "High-accuracy measurement of 240-m distance in an optical tunnel by use of a compact femtosecond laser," Appl. Opt. **39**(30), 5512–5517 (2000).
2. J. Ye, "Absolute measurement of a long, arbitrary distance to less than an optical fringe," Opt. Lett. **29**(10), 1153–1155 (2004).
3. S.-W. Kim, "Photonics metrology: Combs rule," Nat. Photonics **3**(6), 313–314 (2009).
4. G. Wu, M. Takahashi, K. Arai, H. Inaba, and K. Minoshima, "Extremely high-accuracy correction of air refractive index using two-colour optical frequency combs," Sci. Rep. **3**(1), 1894 (2013).
5. T. Dresel, G. Häusler, and H. Venzke, "Three-dimensional sensing of rough surfaces by coherence radar," Appl. Opt. **31**(7), 919–925 (1992).
6. K. Minoshima, H. Matsumoto, Z. Zhang, and T. Yagi, "Simultaneous 3-D imaging using chirped ultrashort optical pulses," Jpn. J. Appl. Phys. **33**(Part 2, No. 9B), L1348–L1351 (1994).
7. T. Kato, M. Uchida, and K. Minoshima, "No-scanning 3D measurement method using ultrafast dimensional conversion with a chirped optical frequency comb," Sci. Rep. **7**(1), 3670 (2017).
8. U. Schnell, S. Gray, and R. Dändliker, "Dispersive white-light interferometry for absolute distance measurement with dielectric multilayer systems on the target," Opt. Lett. **21**(7), 528 (1996).

OSA CONTINUUM

9. C. Dorrer, N. Belabas, J.-P. Likforman, and M. Joffre, "Spectral resolution and sampling issues in Fourier-transform spectral interferometry," J. Opt. Soc. Am. B **17**(10), 1795 (2000).
10. P. Hlubina, D. Ciprian, J. Lunácek, and M. Lesnák, "Dispersive white-light spectral interferometry with absolute phase retrieval to measure thin film," Opt. Express **14**(17), 7678 (2006).
11. C. Iaconis and I. A. Walmsley, "Spectral phase interferometry for direct electric-field reconstruction of ultrashort optical pulses," Opt. Lett. **23**(10), 792 (1998).
12. P. Hlubina, "Dispersive spectral-domain two-beam interference analysed by a fibre-optic spectrometer," J. Mod. Opt. **51**(4), 537–547 (2004).
13. A. Hirai and H. Matsumoto, "Measurement of group refractive index wavelength dependence using a low-coherence tandem interferometer," Appl. Opt. **45**(22), 5614 (2006).
14. P. Hlubina and J. Olszewski, "Phase retrieval from spectral interferograms including a stationary-phase point," Opt. Commun. **285**(24), 4733–4738 (2012).
15. Y. Nakajima and K. Minoshima, "Highly stabilized optical frequency comb interferometer with a long fiber-based reference path towards arbitrary distance measurement," Opt. Express **23**(20), 25979–25987 (2015).
16. H. Matsuoka, Y. Kosai, M. Saito, N. Takeyama, and H. Suto, "Single-cell viability assessment with a novel spectro-imaging system," J. Biotechnol. **94**(3), 299–308 (2002).